Routes to the Quaternary Aluminum Silicides $RE_4Fe_{2+x}Al_{7-x}Si_8$ (RE = Ce, Pr, Nd, Sm); Exploratory Synthesis with Molten Al as a Solvent

B. Sieve,[†] S. Sportouch,[†] X. Z. Chen,[†] J. A. Cowen,[‡,⊥] P. Brazis,[§] C. R. Kannewurf,[§] V. Papaefthymiou,[∥] and M. G. Kanatzidis*[,†]

Department of Chemistry, Michigan State University, East Lansing, Michigan 48824-1322, Department of Physics and Astronomy, Michigan State University, East Lansing, Michigan 48824-1322, Department of Electrical and Computer Engineering, Northwestern University, Evanston, Illinois 60208-3118, and Physics Department, University of Ioannina, Ioannina, Greece 45110

Received June 19, 2000. Revised Manuscript Received October 23, 2000

The four new intermetallic aluminum silicides $RE_4Fe_{2+x}Al_{7-x}Si_8$ (RE = Ce, Pr, Nd, Sm) crystallize from the reaction of Si, Fe, and RE (or rare earth oxides) in molten Al at 850 °C. All compounds share the same structure type as determined by single-crystal X-ray diffraction analysis. They form in the space group *Cmmm* (No. 65) with cell constants of $a = 10.909(2)$ Å, $b = 16.265(3)$ Å, $c = 4.0804(8)$ Å, R1 = 0.0196, and wR2 = 0.0486 for the Sm analogue. The crystal structure is a complex three-dimensional network comprised of repeating layers containing Al, Si, and Fe connected by atoms between the layers. The RE^{3+} ions are then located within tunnels of the three-dimensional network, running parallel to the *c* axis with a coordination number of 14. Magnetic susceptibility measurements indicate that the rare earth ions are in a 3+ oxidation state, whereas the Fe atoms are in an effective diamagnetic state. Electronic band structure calculations, carried out on the hypothetical analogue $Y_4Fe_2Al_7Si_8$, predict metallic behavior and suggest Fe to be in a reduced state with almost filled d orbitals. Variable temperature electrical conductivity and thermopower measurements confirm the metallic nature of the compounds. The charge transport and magnetic properties of the Ce analogue are anomalous and indicative of $f^{1/0}$ valence fluctuations at $T < 100$ K.

Introduction

In recent decades, metal silicides have acquired increasing scientific and technological importance. This class of materials plays a central role in many diverse applications including electrodes for silicon electronic devices,[1] advanced structural materials,[2] aluminum matrix composites,[3] amorphous metals,[4] and so forth. Various review articles and books are available discussing their preparation, properties, structural arrangements,[5] thermodynamics[6] and applications to technology.[7] Traditional synthetic methods rely on direct element combination reactions and require very high temperatures, normally well above 1400 °C, mandating the use of induction heating, arc-melting methods, or other high-energy means. This is needed to facilitate solid-state diffusion. Normally, under such conditions only the thermodynamically favored phases form, often simple binary or ternary compounds, making it difficult to systematically explore possible complex intermetallic phases. A second limitation is that normally only polycrystalline products are formed, although single crystals have occasionally been obtained by annealing or other crystal growth methods. These powders often limit proper and thorough analysis and characterization.

The use of molten fluxes, such as Al and Ga, can greatly reduce the reaction temperatures by removing the need of solid-state diffusion due to the dissolving properties of the flux. While approaches exploiting such molten metals have been used to grow large crystals of known compounds such as the growth of UAl_3 within molten Al,[8] their use in *exploratory synthesis* has been relatively limited. The formation of several novel ter-

* To whom correspondence should be addressed. E-mail: kanatzid@cem.msu.edu.
[†] Department of Chemistry, Michigan State University.
[‡] Department of Physics and Astronomy, Michigan State University.
[§] Northwestern University.
[∥] University of Ioannina.
[⊥] Deceased.

(1) Maex, K. *Mater. Sci. Eng. B* **1993**, *11*, 53−153. (b) Muraka, S. P. *Silicides for VLSI Applications*; Academic Press: New York, 1983.
(2) Shah, D. M.; Berczik, D.; Anton, D. L.; Hecht, R. *Mater. Sci. Eng. A* **1992**, *155*, 45−57.
(3) Ochiai, S. *Mechanical Properties of Metallic Composites*; Marcel Dekker: New York, 1994. (b) Suresh, S.; Mortensen, A.; Needleman, A. *Fundamentals of Metal Matrix Composites*; Butterworth-Heinemann: Boston, 1993.
(4) Mizushima, T.; Ikarashi, K.; Yoshida, S.; Makino A.; Inoue, A. *Mater. Trans. JIM* **1999**, *40*, 1019−1022. (b) Chiriac, H.; Lupu, N. *J. Non-Cryst. Solids* **1999**, *252*, 751−756.
(5) Aronsson, B.; Lundström, T.; Rundqvist, S. *Borides, Silicides and Phosphides*; Methuen & Co. Ltd.: London, 1965.
(6) Schlesinger, M. E. *Chem. Rev.* **1990**, *90*, 607−628. (b) Chart, T. G. *A Critical Assessment of Thermochemical Data for Transition Metal-Silicon Systems*; NPL Report on Chemistry 18; National Physical Laboratory: Teddington, U.K., 1972.
(7) Reader, A. H.; Vanommen, A. H.; Weijs, P. J. W.; Wolters, R.; Oostra, D. J. *Rep. Prog. Phys.* **1993**, *56* (11), 1397−1467. (b) Maex, K. *Appl. Surf. Sci.* **1991**, *53*, 328−337.
(8) Fisk, Z.; Remeika, J. P. *Handbook on the Physics and Chemistry of Rare Earths*; Gschneidner, K. A., Jr., Eyring, L., Eds.; North-Holland Publishing Co.: Amsterdam, The Netherlands, 1995; Vol. 21.

10.1021/cm0004937 CCC: $20.00
Published on Web 01/17/2001

nary and quaternary compounds from molten metal fluxes in recent years, however, has highlighted new possibilities of such methods in exploratory work.[9]

With this in mind, we have recently initiated exploratory studies of silicide and germanide compounds using liquid Al and Ga as solvents. Our aim is to develop moderate temperature synthetic routes to a wide range of novel intermetallic solids. Molten Al and Ga are particularly suited to the study of reactions of Si and Ge because no compounds of binary combinations exist for these elements.[10] We find that, indeed, many new compounds containing tetrelides (i.e., group 14 element containing compounds) form within the molten Al and Ga flux at lower temperatures. We have reported already the formation of silicides such as $Ho_2Al_3Si_2$[9a] and $Sm_2Ni(Ni_xSi_{1-x})Al_4Si_6$[11] along with germanides such as $SmNiAl_4Ge_2$.[12] In addition, the syntheses of the ternary silicide $SmNiSi_3$[13] and the gallide Sm_2NiGa_{12}[14] from molten Ga have been described elsewhere.

So far, we focused our investigations on the Ni systems and we were surprised to learn from these studies that Ni is actually reduced in these phases, achieving a diamagnetic d^{10} electronic configuration. The additional electron density seems to originate from the more electropositive RE and Al atoms in the structure. Because the neighboring transition metals Mn, Fe, and Co have similar electronegativity to Ni but different electron counts, we decided to comparatively study the corresponding RE/Mn/Al/Si, RE/Fe/Al/Si, and RE/Co/Al/Si[15] systems. We are particularly interested in the electron donor/acceptor behavior of these transition metals as well as the effects they have on both the composition and structure of their quaternary intermetallics. The nature of the transition metals influences the chemistry and can lead to a variety of new structures and properties.

Reports of quaternary Fe intermetallic compounds in the literature are relatively scarce. These studies have mostly concentrated on the substitution of known ternaries, forming pseudo-ternaries of known structure types as in $Sm_2Fe_{14-x}Co_xAl_3$ of the Th_2Zn_{17} structure type,[16] or investigations of quaternary Fe quasi-crystalline materials such as those formed in the alloys of Al−Cu−Co−Fe.[17] Here, we report results on the RE/Fe/Al/Si system, namely, the synthesis, structure, electronic band structure calculations, Mössbauer spectroscopy, electrical properties, and magnetic properties of the novel series of compounds $RE_4Fe_{2+x}Al_{7-x}Si_8$ (RE = Ce, Pr, Nd, Sm) that feature a novel structure type.

Experimental Section

Reagents. The following reagents were used as obtained: Ce, Nd, and Sm, 99.9%, metal chips, Research Chemicals, Phoenix, AZ; Pr, 99.9%, −40 mesh, Cerac, Milwaukee, WI; CeO_2, Pr_6O_{11} and Nd_2O_3, Sylvania, Towanda, PA; Sm_2O_3, Rhone-Poulenc, Princeton NJ; Fe, 99.99%, fine powder, Aldrich Chemical, Milwaukee, WI; Si, 99.96%, −325 mesh, Cerac, Milwaukee, WI; Al, 20 mesh, Fisher, Fair Lawn, NJ.

Synthesis. We explored two synthetic methods in the synthesis of the title compounds. One uses elemental RE as the starting materials while the other uses the corresponding RE oxides.

Method A. $RE_4Fe_{2+x}Al_{7-x}Si_8$ was prepared by mixing 0.0335 g (0.6 mmol) of Fe metal, 1.2 mmol of elemental rare earth, 0.243 g (9.0 mmol) of Al, and 0.0674 g (2.4 mmol) of Si in a nitrogen atmosphere and placed in an alumina tube. The alumina tube was then sealed in an evacuated (1.0×10^{-4} Torr) 13-mm o.d. × 11-mm i.d. fused silica tube and heated at 850 °C for 4 days. The tube was then cooled to 500 °C in 3 days (−4.86 °C/h) and finally to 50 °C in 12 h (−37.5 °C/h). The final products were isolated from the solidified Al matrix with 5 M NaOH solution. After the Al matrix was removed, the product was washed and dried using acetone and ether. The products were then submerged in a 50% HCl solution (by volume) for 30 min to remove any acid-soluble byproducts. The final isolation, after drying, yielded stable silver needles or rods and black powder, both of the desired phase, in 40% yield based on the rare earth component. The purity of the final product was confirmed through comparison of the experimental X-ray diffraction powder patterns, taken of the bulk product, to theoretical patterns calculated from the refined single-crystal data.

Method B. With the oxide starting materials, the title compounds were prepared by mixing 0.0335 g (0.6 mmol) of Fe metal, 1.2 mmol of rare earth ion in oxide form, 0.243 g (9.0 mmol) of Al, and 0.0674 g (2.4 mmol) of Si and placing them in an alumina tube. The alumina tube was then sealed in an evacuated (1.0×10^{-4} Torr) 13-mm o.d. × 11-mm i.d. fused silica tube and heated at 850 °C for 4 days. The tube was then cooled to 500 °C in 3 days (−4.86 °C/h) and finally to 50 °C in 12 h (−37.5 °C/h). The products of method B were isolated by the same means as those in method A. In contrast to method A, sample preparation for method B was performed under an oxygen atmosphere.

Slight differences in crystal quality exist between the two synthesis methods. $RE_4Fe_{2+x}Al_{7-x}Si_8$ crystals grown from oxide starting materials were fewer but of better quality, often growing larger than 0.5 mm and exhibiting facetted edges. On the other hand, reactions employing elemental rare earths produced many more crystals; however, these were of poorer quality, smaller, and often twinned.

EDS Analysis. Semiquantitative microprobe analyses of the compounds were performed with a JEOL JSM-35C scanning electron microscope (SEM) equipped with a Noran Vantage detector. Data were acquired using an accelerating voltage of 25 kV and a 100-s accumulation time on several crystals. Crystals from both synthetic methods were analyzed, yielding a consistent elemental ratio of approximately "$RE_2FeAl_{3.5}Si_4$".

Single-Crystal X-ray Crystallography. Data on $Sm_4Fe_{2+x}Al_{7-x}Si_8$ and $Ce_4Fe_{2+x}Al_{7-x}Si_8$ were collected using a Rigaku AFC6S four-circle automated diffractometer. Data were collected at room temperature using Mo Kα (λ = 0.71073 Å) radiation. An empirical absorption correction was made based on Ψ scans. The structures were solved with direct methods

(9) $Ho_2Al_3Si_2$: Chen, X. Z.; Sieve, B.; Henning, R.; Schultz, A. J.; Brazis, P.; Kannewurf, C. R.; Cowen, J. A.; Crosby R.; Kanatzidis, M. G. *Angew. Chem., Int. Ed.* **1999**, *5*, 693−696. (b) RET_2Al_{20}: Niemann, S.; Jeitschko, W. J. *J. Solid State Chem.* **1995**, *114*, 337−341. (c) $PrRh_{4.8}B_2$: Shishido, T.; Oku, M.; Higashi, I.; Okada, S.; Kudou, K.; Asami, K.; Horiuchi, H.; Fukuda, T. *J. Ceram. Soc. Jpn.* **1999**, *107*, 1087−1092.

(10) *Binary Alloy Phase Diagrams*; Massalski, T. B., Ed.; American Society for Metals: Metals Park, OH, 1986.

(11) Chen, X. Z.; Sportouch, S.; Sieve, B.; Brazis, P.; Kannewurf, C. R.; Cowen, J. A.; Patschke, R.; Kanatzidis, M. G. *Chem. Mater.* **1998**, *10*, 3202−3211.

(12) Sieve, B.; Chen, X.; Cowen, J.; Larson, P.; Mahanti, S. D.; Kanatzidis, M. G. *Chem. Mater.* **1999**, *11*, 2451−2455.

(13) Chen, X. Z.; Larson, P.; Sportouch, S.; Brazis, P.; Mahanti, S. D.; Kannewurf, C. R.; Kanatzidis, M. G. *Chem. Mater.* **1998**, *11*, 75−83.

(14) Chen, X. Z.; Small, P.; Sportouch S.; Zhuravleva, M.; Brazis, P.; Kannewurf, C. R.; Kanatzidis, M. G. *Chem. Mater.*, submitted.

(15) Our results on the RE/Mn/Al/Si and Re/Co/Al/Si systems will be published elsewhere.

(16) Wang, Z.; Dunlap, R. A.; Foldeaki, M. *J. Mater. Sci.* **1994**, *29*, 5333−5336.

(17) Perez, R.; Juarezislas, J. A.; Martinez, L. *Mater. Sci. Eng. A* **1994**, *182*, 837−840.

Table 1. Crystallographic Data for $RE_4Fe_{2+x}Al_{7-x}Si_8$ (RE = Ce, Pr, Nd, Sm)

	compound			
	$Ce_4Fe_{2+x}Al_{7-x}Si_8$	$Pr_4Fe_{2+x}Al_{7-x}Si_8$	$Nd_4Fe_{2+x}Al_{7-x}Si_8$	$Sm_4Fe_{2+x}Al_{7-x}Si_8$
formula weight	1093.26	1096.92	1109.74	1134.18
crystal size (mm)	0.06 × 0.03 × 0.03	0.07 × 0.04 × 0.04	0.1 × 0.04 × 0.04	0.22 × 0.1 × 0.1
a (Å)	10.936(2)	10.893(2)	10.898(4)	10.909(2)
b (Å)	16.404(3)	16.305(3)	16.315(11)	16.265(3)
c (Å)	4.1532(8)	4.1290(8)	4.1310(14)	4.0804(8)
V (Å^3)	745.1(3)	733.3(3)	734.5(6)	724.0(3)
Z	2	2	2	2
space group	*Cmmm* (No. 65)	*Cmmm* (No. 65)	*Cmmm* (No. 65)	*Cmmm* (No. 65)
d_{calc} (g cm^{-3})	4.873	4.965	5.018	5.203
temperature (K)	298	273	298	298
2θ range (deg)	4.48−56.50	8.38−62.56	4.5−56.44	4.50−59.80
radiation	Mo Kα (λ = 0.71069 Å)	Mo Kα (λ = 0.71069 Å)	Mo Kα (λ = 0.71069 Å)	Mo Kα (λ = 0.71069 Å)
collection system	Rigaku 4 Circle	Siemens CCD	Siemens CCD	Rigaku 4 Circle
frame collection time	n/a	20 s	20 s	n/a
kV/mA	50/40	50/40	34/40	40/30
μ (mm^{-1})	15.115	16.230	17.075	19.202
index ranges	$-14 \le h \le 14$ $-21 \le k \le 21$ $-5 \le l \le 5$	$-15 \le h \le 15$ $-22 \le k \le 23$ $-5 \le l \le 5$	$-14 \le h \le 14$ $-21 \le k \le 21$ $-5 \le l \le 5$	$0 \le h \le 15$ $0 \le k \le 22$ $-1 \le l \le 5$
reflections collected	3708	4393	3612	642
unique reflections	555 (R_{int}= 0.0263)	677 (R_{int}= 0.0395)	556 (R_{int}= 0.0324))	641 (unique data only)
R1/wR2 ($I > 2\sigma$)	0.0196/0.0486	0.0286/0.0748	0.0192/0.0420	0.0207/0.0504
R1/wR2 (all data)	0.0225/0.0597	0.0287/0.0749	0.0249/0.0437	0.0225/0.0510
G.O.F. on F^2	1.146	1.320	1.106	1.256
max. peak and hole (e Å^{-3})	1.642/−1.118	2.241/−1.623	1.401/−1.062	1.279/−1.947
extinction coefficient	0.00188(16)	0.0025(2)	0.00324(15)	0.0057(3)

and refined using the SHELXL software.[18] For these compounds, as with all Al/Si compounds, the Al and Si positions could not be distinguished directly due to Al and Si's similar X-ray scattering lengths. The identification of Al and Si atoms was then made through analysis and careful consideration of the bond distances involving a particular site. This will be discussed further later.

Single-crystal X-ray analysis was completed on the other homologues using a Siemens SMART Platform CCD diffractometer with Mo Kα radiation. Cell refinement and data processing were performed using the program SAINT.[19] A semiempirical absorption correction was applied with the use of the SADABS program.[20] The final structure was solved and refined with SHELXL[18] using the $Sm_4Fe_{2+x}Al_{7-x}Si_8$ coordinates as a basis. Table 1 gives the crystallographic and refinement data for the structural analogues, whereas Tables 2 and 3 give the atomic positions and anisotropic temperature factors, respectively. Selected bond distances and angles for the Sm analogue are shown in Tables 4 and 5.

An unexpected result was the discovery of one site in the structure (M(1), Wyckoff position 2d) exhibiting mixed occupancy between Al and Fe. After an initial structural solution for each analogue was completed, several more crystals of each RE analogue were examined to study the variability of the Fe/Al occupancy in the M(1) site. It was found that for the earlier rare earths of the series (RE = Ce, Pr, Nd) only a small percentage (<10%) of the Al was replaced by Fe on the M(1) site, whereas the analogue with the smallest rare earth, Sm, consistently exhibited higher disorder with values between 15 and 25% Fe substitution on the site. The reasons for the larger extent of disorder are as of yet unknown but they could derive from subtle steric effects associated with the relative RE atomic sizes. Crystals selected from the two different synthetic methods showed no significant differences in their final refined Al/Fe occupancy ratio.

Electronic Structure. The crystal structures of $RE_4Fe_{2+x}Al_{7-x}Si_8$ for RE = Ce, Nd, Pr, and Sm possess a disordered site between Al and Fe atoms. Indeed, Al atoms occupy over 84% of this site. Consequently, because a mixed site cannot be easily described in extended Hückel tight binding theory, we performed an electronic structure calculation assuming the 2d Wyckoff site as fully occupied by Al. In addition, all rare earth elements involved in this series of compounds possess an incomplete f shell. The 4f orbitals are closely localized within the rare earth electron core and therefore the 4f electrons interact much more strongly with each other (i.e., electronic repulsion) than with the electrons of the neighboring atoms. In contrast, the remaining electrons belonging to the rare earth valence (5d, 6s, 6p) orbitals strongly mix with those of the surrounding atoms. Consequently, the 4f orbitals were not included in the electronic structure calculations. As discussed elsewhere,[21] one way to avoid the f orbitals in the calculations is to use a Y atom to mimic the rare earth elements. Y possesses no f shell and its orbital energies are similar to those of the Ce,[22] Pr,[23] and Sm[22] atoms. Therefore, the electronic structure performed on the theoretical compound $Y_4Fe_2Al_7Si_8$, using the program package CAESAR 1.0,[24,25] is considered adequate for representing the compounds presented in this paper. The atomic orbital parameters, that is, energies and exponents, used in the Slater-type wave functions were chosen from one of the three databases available in the CEASAR package and are given in Table 6.[26−29] The nondiagonal Hamiltonian matrix elements were computed with the modified Wolfsberg−Helmohtz formula.[30] The number of electrons corresponding to the Fermi level will be 162 for the

(18) Sheldrick, G. M. *SHELXL. Structural Determination Programs*, Version 5.0; Siemens Analytical X-ray Instruments Inc.: Madison, WI, 1995.
(19) *SAINT*, version 4; Siemens Analytical X-ray Instruments Inc.: Madison, WI, 1998.
(20) Sheldrick, G. M. University of Göttingen, Germany, to be published.
(21) Nordell, K. J.; Miller, G. J. *Angew. Chem., Int. Ed. Engl.* **1997**, *36*, 2008−2010.
(22) Ortiz, J. V.; Hoffmann, R. *Inorg. Chem.* **1985**, *24*, 2095−2104.
(23) Tian, Y. C.; Hughbanks, T. *Inorg. Chem.* **1993**, 32, 400−405.
(24) Whangbo, M.-H.; Hoffmann, R. *J. Am. Chem. Soc.* **1978**, *100*, 6093−6098.
(25) Ren, J.; Liang, W.; Whangbo, M.-H. *Crystal and Electronic Structure Analysis Using CAESAR*; PrimeColor Software, Inc.: NC, 1998.
(26) H_{ii} values are taken from the CAESAR package database.
(27) Summerville, R. H.; Hoffmann, R. *J. Am. Chem. Soc.* **1976**, *98*, 7240−7254.
(28) Trong Anh, N.; Elian, M.; Hoffmann, R. *J. Am. Chem. Soc.* **1978**, *100*, 110−116.
(29) Anderson, A. B.; Hoffmann, R. *J. Chem. Phys.* **1974**, *60*, 4271−4273.
(30) Ammeter, J.; Bürgi, H.-B.; Tibeault, J.; Hoffmann, R. *J. Am. Chem. Soc.* **1978**, *100*, 3686−3692.

Table 2. Atomic Coordinates and Equivalent IsotropicDisplacement Parameters ($A^2 \times 10^3$) for $RE_4Fe_{2+x}Al_{7-x}Si_8$ (RE = Ce, Nd, Pr, Sm)[a]

	Wyckoff position	*x*	*y*	*z*	*U*(eq)	occ.
Ce	8q	0.2687(1)	0.1293(1)	1/2	4(1)	1
Pr		0.2681(1)	0.1293(1)	1/2	5(1)	1
Nd		0.2683(1)	0.1295(1)	1/2	4(1)	1
Sm		0.2672(1)	0.1292(1)	1/2	8(1)	1
Fe	4i	0	0.1336(1)	0	4(1)	1
		0	0.1339(1)	0	4(1)	1
		0	0.1342(1)	0	4(1)	1
		0	0.1350(1)	0	6(1)	1
Si(1)	8p	0.1410(1)	0.2443(1)	0	5(1)	1
		0.1413(2)	0.2446(1)	0	6(1)	1
		0.1416(1)	0.2446(1)	0	5(1)	1
		0.1418(1)	0.2456(1)	0	7(1)	1
Si(2)	4j	0	0.0731(1)	1/2	5(1)	1
		0	0.0729(1)	1/2	5(1)	1
		0	0.0729(1)	1/2	4(1)	1
		0	0.0731(1)	1/2	7(1)	1
Si(3)	4g	0.3494(2)	0	0	6(1)	1
		0.3492(2)	0	0	7(1)	1
		0.3487(2)	0	0	5(1)	1
		0.3497(2)	0	0	11(1)	1
Al(1)	4i	1/2	0.1243(1)	0	9(1)	1
		1/2	0.1240(2)	0	11(1)	1
		1/2	0.1241(1)	0	9(1)	1
		1/2	0.1228(1)	0	25(1)	1
Al(2)	4g	0.1212(2)	0	0	7(1)	1
		0.1212(3)	0	0	7(1)	1
		0.1211(2)	0	0	6(1)	1
		0.1224(3)	0	0	8(1)	1
Al(3)	4j	0	0.2338(1)	1/2	6(1)	1
		0	0.2341(2)	1/2	6(1)	1
		0	0.2344(1)	1/2	6(1)	1
		0	0.2355(1)	1/2	8(1)	1
M(1)	2d	1/2	0	1/2	8(1)	0.973 Al + 0.027 Fe
		1/2	0	1/2	9(1)	0.960 Al + 0.040 Fe
		1/2	0	1/2	8(1)	0.993 Al + 0.006 Fe
		1/2	0	1/2	7(1)	0.838 Al + 0.162 Fe

[a] *U*(eq) is defined as one-third of the trace of the orthogonalized U_{ij} tensor.

hypothetical Y compound as well as for the Ce, Nd, Pr, and Sm analogues. Attempts to form the Y analogue discussed below have to date failed, instead yielding a hexagonal quaternary compound.[31]

Mössbauer Spectroscopy. Mössbauer measurements were performed on $RE_4Fe_{2+x}Al_{7-x}Si_8$ RE = Ce and Pr in transmission geometry between 4.2 and 300 K using a ^{57}Co(Rh) source and conventional methods. Isomer shifts are reported relative to iron metal at room temperature (300 K). The least-squares fit gave a slightly asymmetric doublet with the intensity of the low-speed line lower than that of the high-speed line. The asymmetry is more pronounced in the case of the Pr compound, and it is constant versus temperature. Taking this into account, and the fact that the line widths of the Lorentzian lines are the expected ones (for our experimental set-up) and equal for both lines of the quadruple doublet, we conclude that the asymmetry is most likely due to texture effects.

Electrical and Magnetic Properties. We performed dc electrical conductivity and thermopower measurements on selected single-crystal samples using techniques described elsewhere.[32,33]

(31) The results of the Y/Fe/Al/Si system will be published elsewhere.

Table 3. Anisotropic Displacement Parameters ($A^2 \times 10^3$) for $RE_4Fe_{2+x}Al_{7-x}Si_8$ (RE = Ce, Pr, Nd, Sm)[a]

	U_{11}	U_{22}	U_{33}	U_{23}	U_{13}	U_{12}
Ce	4(1)	5(1)	4(1)	0	0	0
Pr	8(1)	4(1)	4(1)	0	0	0
Nd	4(1)	3(1)	5(1)	0	0	0
Sm	9(1)	5(1)	10(1)	0	0	0
Fe	4(1)	4(1)	4(1)	0	0	0
	7(1)	3(1)	3(1)	0	0	0
	5(1)	3(1)	4(1)	0	0	0
	6(1)	4(1)	7(1)	0	0	0
Si(1)	3(1)	7(1)	6(1)	0	0	0
	6(1)	6(1)	6(1)	0	0	−1
	5(1)	5(1)	6(1)	0	0	0
	5(1)	6(1)	10(1)	0	0	0
Si(2)	4(1)	6(1)	4(1)	0	0	0
	8(1)	4(1)	4(1)	0	0	0
	6(1)	3(1)	3(1)	0	0	0
	9(1)	6(1)	8(1)	0	0	0
Si(3)	4(1)	6(1)	9(1)	0	0	0
	7(1)	4(1)	10(1)	0	0	0
	4(1)	4(1)	8(1)	0	0	0
	6(1)	4(1)	22(1)	0	0	0
Al(1)	3(1)	6(1)	18(1)	0	0	0
	7(1)	5(1)	23(2)	0	0	0
	4(1)	6(1)	17(1)	0	0	0
	6(1)	5(1)	64(2)	0	0	0
Al(2)	4(1)	7(1)	8(1)	0	0	0
	5(1)	7(1)	11(1)	0	0	0
	3(1)	6(1)	8(1)	0	0	0
	4(1)	7(1)	14(1)		0	0
Al(3)	6(1)	7(1)	6(1)	0	0	0
	7(1)	7(1)	5(1)	0	0	0
	4(1)	6(1)	9(1)	0	0	0
	4(1)	9(1)	10(1)	0	0	0
M(1)	8(1)	9(1)	8(1)	0	0	0
	9(2)	9(2)	9(2)	0	0	0
	8(1)	7(1)	9(2)	0	0	0
	3(1)	7(1)	11(1)	0	0	0

[a] The anisotropic displacement factor exponent takes the following form: $-2\pi^2[h^2a^{*2}U_{11} + ... + 2hka^*b^*U_{12}]$.

Table 4. Selected Bond Lengths (Å) for $Sm_4Fe_{2+x}Al_{7-x}Si_8$

bond	distance (Å)	number present	bond	distance (Å)	number present
Sm−Si(1)	3.0484(10)	2	Fe−Al(3)	2.6151(14)	2
Sm−Si(2)	3.0541(8)	1	M(1)−Si(3)	2.6171(12)	4
Sm−Si(3)	3.0640(7)	2	M(1)−Al(1)	2.8546(14)	4
Sm−Si(1)	3.1017(10)	2	Si(1)−Si(1)	2.364(2)	1
Sm−Al(1)	3.2595(5)	2	Si(1)−Al(3)	2.5658(8)	2
Sm−M(1)	3.2963(5)	1	Si(1)−Al(1)	2.641(2)	2
Sm−Al(2)	3.3276(10)	2	Si(2)−Si(2)	2.377(3)	1
Sm−Al(3)	3.360(1)	1	Si(2)−Al(3)	2.643(2)	1
Sm−Al(3)	3.389(1)	1	Si(2)−Al(2)	2.7122(13)	4
Fe−Si(2)	2.2751(9)	2	Si(3)−Al(2)	2.481(3)	1
Fe−Si(1)	2.3739(14)	2	Si(3)−Al(1)	2.5833(19)	2
Fe−Al(2)	2.5690(13)	2	Al(2)−Al(2)	2.669(4)	1

Magnetic susceptibility for $RE_4Fe_{2+x}Al_{7-x}Si_8$ (RE = Ce, Pr, Sm, Nd) were measured as a function of temperature using a MPMS Quantum Design SQUID magnetometer. A linear field dependence of the magnetization was observed. The measurements on polycrystalline samples were done under increasing temperature with a 200-G applied field.

Results and Discussion

Synthesis. The combination of rare earth elements, transition metals, and silicon in excess molten Al conveniently gives large crystals of ternary and qua-

(32) Lyding, J. W.; Marcy, H. O.; Marks, T. J.; Kannewurf, C. R. *IEEE Trans. Meas.* **1988**, *37*, 76−80.
(33) Marcy, H. O.; Marks, T. J.; Kannewurf, C. R. *IEEE Trans. Instrum. Meas.* **1990**, *39*, 756−760.

Table 5. Selected Bond Angles in Degrees for $Sm_4Fe_{2+x}Al_{7-x}Si_8$

Si(1)−Sm−Si(1)	84.02(3)	Si(1)−Si(1)−Fe	134.10(8)
Si(1)−Sm−Si(2)	120.69(3)	Si(1)−Si(1)−Al(3)	127.28(2)
Si(1)−Sm−Si(3)	85.21(3)	Fe−Si(1)−Al(3)	63.79(4)
Si(1)−Sm−Si(3)	143.89(4)	Al(3)−Si(1)−Al(3)	105.34(5)
Si(2)−Sm−Si(3)	94.34(4)	Si(1)−Si(1)−Al(1)	122.43(8)
Si(3)−Sm−Si(3)	83.50(2)	Fe−Si(1)−Al(1)	103.46(5)
Si(1)−Sm−Si(1)	45.20(4)	Al(3)−Si(1)−Al(1)	72.46(5)
Si(1)−Sm−Si(1)	100.13(2)	Fe−Si(2)−Fe	127.47(8)
Si(2)−Sm−Si(1)	76.22(3)	Fe−Si(2)−Si(2)	116.26(4)
Si(3)−Sm−Si(1)	96.34(3)	Fe−Si(2)−Al(3)	63.74(4)
Si(3)−Sm−Si(1)	170.53(4)	Si(2)−Si(2)−Al(3)	180.0
Si(1)−Sm−Si(1)	82.26(3)	Fe−Si(2)−Al(2)	150.28(4)
Si(1)−Sm−Al(1)	49.36(4)	Fe−Si(2)−Al(2)	61.27(2)
Si(1)−Sm−Al(1)	100.75(3)	Si(2)−Si(2)−Al(2)	64.01(3)
Si(2)−Sm−Al(1)	137.23(2)	Al(3)−Si(2)−Al(2)	115.99(3)
Si(3)−Sm−Al(1)	48.10(4)	Fe−Si(2)−Al(2)	150.28(4)
Si(3)−Sm−Al(1)	99.54(4)	Al(2)−Si(2)−Al(2)	58.96(7)
Si(1)−Sm−Al(1)	87.21(3)	Al(2)−Si(2)−Al(2)	97.57(6)
Si(1)−Sm−Al(1)	140.78(4)	Al(2)−Si(2)−Al(2)	128.03(6)
Al(1)−Sm−Al(1)	77.499(17)	Al(2)−Si(3)−Al(1)	129.38(4)
Si(1)−Sm−M(1)	100.06(3)	Al(1)−Si(3)−Al(1)	101.23(8)
Si(2)−Sm−M(1)	123.01(3)	Al(2)−Si(3)−M(1)	128.78(3)
Si(3)−Sm−M(1)	48.43(3)	Al(1)−Si(3)−M(1)	66.58(4)
Si(1)−Sm−M(1)	136.799(17)	M(1)−Si(3)−M(1)	102.44(6)
Al(1)−Sm−M(1)	51.62(3)	Si(3)−Al(1)−Si(3)	78.77(8)
Si(1)−Sm−Al(2)	99.55(2)	Si(3)−Al(1)−Si(1)	176.48(6)
Si(1)−Sm−Al(2)	170.62(4)	Si(3)−Al(1)−Si(1)	104.75(5)
Si(2)−Sm−Al(2)	50.08(3)	Si(1)−Al(1)−Si(1)	71.73(7)
Si(3)−Sm−Al(2)	45.44(5)	Si(3)−Al(1)−M(1)	57.27(4)
Si(3)−Sm−Al(2)	96.60(2)	Si(1)−Al(1)−M(1)	124.530(17)
Si(1)−Sm−Al(2)	76.88(3)	M(1)−Al(1)−M(1)	91.24(6)
Si(1)−Sm−Al(2)	125.43(4)	Si(3)−Al(2)−Fe	121.30(4)
Al(1)−Sm−Al(2)	88.05(4)	Fe−Al(2)−Fe	117.40(8)
Al(1)−Sm−Al(2)	137.18(4)	Si(3)−Al(2)−Al(2)	180.0
Si(2)−Fe−Si(2)	127.47(8)	Fe−Al(2)−Al(2)	58.70(4)
Si(2)−Fe−Si(1)	109.61(3)	Si(3)−Al(2)−Si(2)	119.48(4)
Si(1)−Fe−Si(1)	81.35(7)	Fe−Al(2)−Si(2)	50.95(3)
Si(2)−Fe−Al(2)	67.78(4)	Fe−Al(2)−Si(2)	96.82(6)
Si(1)−Fe−Al(2)	170.63(5)	Al(2)−Al(2)−Si(2)	60.52(4)
Si(1)−Fe−Al(2)	108.02(5)	Si(2)−Al(2)−Si(2)	51.97(6)
Al(2)−Fe−Al(2)	62.60(8)	Si(2)−Al(2)−Si(2)	97.57(6)
Si(2)−Fe−Al(3)	64.99(5)	Si(2)−Al(2)−Si(2)	121.04(7)
Si(2)−Fe−Al(3)	167.54(6)	Si(1)−Al(3)−Si(1)	105.34(5)
Si(1)−Fe−Al(3)	61.68(3)	Si(1)−Al(3)−Si(1)	74.17(5)
Al(2)−Fe−Al(3)	122.31(3)	Si(1)−Al(3)−Si(1)	172.65(10)
Al(3)−Fe−Al(3)	102.55(7)	Si(1)−Al(3)−Fe	54.53(3)
Si(3)−M(1)−Si(3)	180.0	Si(1)−Al(3)−Fe	131.33(6)
Si(3)−M(1)−Si(3)	77.56(6)	Fe−Al(3)−Fe	102.55(7)
Si(3)−M(1)−Si(3)	102.44(6)	Si(1)−Al(3)−Si(2)	93.68(5)
Si(3)−M(1)−Al(1)	56.14(3)	Fe−Al(3)−Si(2)	51.28(4)
Si(3)−M(1)−Al(1)	123.86(3)		
Al(1)−M(1)−Al(1)	91.24(6)		
Al(1)−M(1)−Al(1)	180.0		
Al(1)−M(1)−Al(1)	88.76(6)		

ternary compounds, often exhibiting interesting new structural arrangements. Liquid Al is an excellent solvent for various metals and Si. Because of the eutectic nature of the Si/Al interaction,[10] a large amount of Si can be dissolved and remain highly reactive in liquid Al. The presence of dissolved Si then creates excellent reaction conditions with other elements, even if these elements themselves are only present in small percentages or dissolve only partially. Crystals of $RE_4Fe_{2+x}Al_{7-x}Si_8$ (RE = Ce, Pr, Nd, Sm) grow from liquid Al as large needlelike crystals (see Figure 1).

The Al flux also permits the use of metal oxide starting materials, which decreases costs and allows reactant handling in ambient atmosphere. When a metal oxide precursor is used, the Al acts not only as a flux but also as a reducing agent. A powerful force, the formation of Al_2O_3 drives this reduction, in a process reminiscent of the thermite reaction.[34]

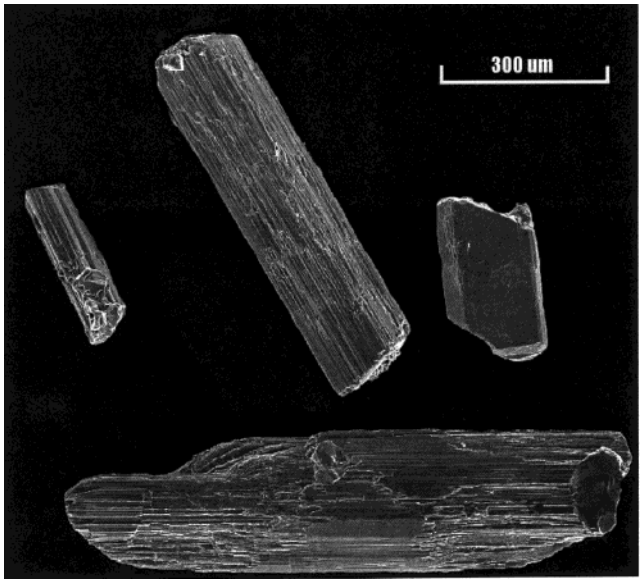

Figure 1. SEM image of crystals of $Sm_4Fe_{2+x}Al_{7-x}Si_8$ exhibiting typical rodlike morphology.

Table 6. Exponents and Parameters Used in the Extended Hückel Calculations (The Contraction Coefficients Used in the Double-ζ Expansion Are c_1 and c_2)

atoms	orbitals	H_{ii} (eV)	ζ_1	c_1	ζ_2	c_2	reference
Y	5s	−6.81	1.6	0.55	0.95	0.5686	26
	5p	−3.76					
	4d	−6.10					
Fe	4s	−9.1	1.9	1.0			26, 27
	4p	−5.32	1.9	1.0			
	3d	−12.60	5.35	0.55	2.0	0.626	
Si	3s	−17.299	1.383	1.0			26, 28
	3p	−9.20	1.383	1.0			
Al	3s	−12.30	1.167	1.0			26, 29
	3p	−6.50	1.167	1.0			

Therefore, larger quantities of Al are recommended to compensate for the formation of Al_2O_3. The Al reduces the starting oxide materials into dispersed fine particles of reactive metal. The presence of highly dispersed metal particles then allows reactions to occur at lower temperatures than otherwise would as described previously in the synthesis of $Sm_2Ni(Ni_xSi_{1-x})Al_4Si_6$.[11]

Structure Description. The $RE_4Fe_{2+x}Al_{7-x}Si_8$ (RE = Ce, Pr, Nd, Sm) series adopts a new structure type in the space group *Cmmm* (No. 65). The compounds exhibit a complex three-dimensional Fe−Al−Si framework with small channels running parallel to the *c* axis, which contain the rare earth ions (see Figure 2).

Before we discuss the structure in any detail, we address the issue of distinguishing between Al and Si. As mentioned earlier, the atomic assignments of Si and Al positions can be made readily based on bond distances. This was shown by subsequent neutron diffraction analysis to be reliable in the Al and Si assignments for similar intermetallic compounds.[9a] On the basis of their relative atomic sizes and different individual chemical properties, bonds involving Si are significantly shorter than those of Al. For example, in $Sm_4Fe_{2+x}Al_{7-x}Si_8$ the Sm−Si distances range from 3.048(1) to

(34) Nebergall, W.; Schmidt, F.; Holtzclaw, H., Jr. *General Chemistry*; D. C. Health and Co.: Lexington, 1972; p 845.

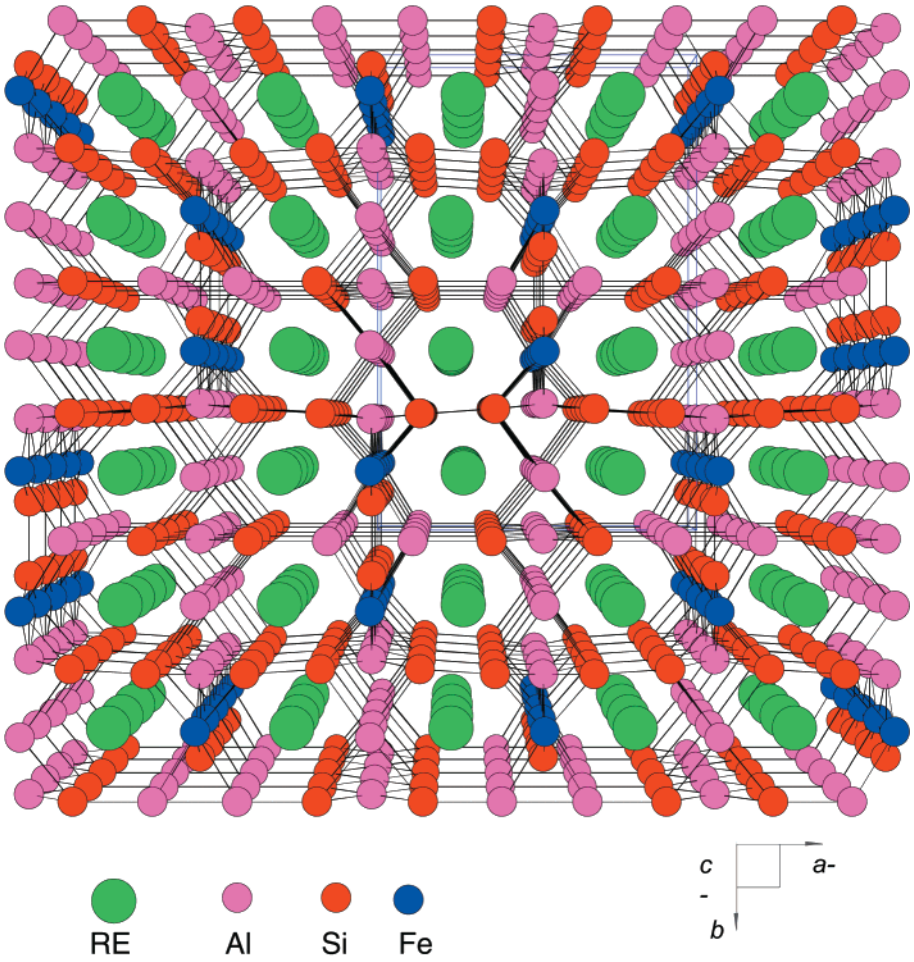

Figure 2. Structure of $RE_4Fe_{2+x}Al_{7-x}Si_8$ (RE = Ce, Nd, Pr, Sm) viewed down the *c* axis.

3.102(1) Å whereas the Sm−Al distances range from 3.259(1) to 3.328(1) Å. These assignments also agree with the Fe distances of 2.275(1)−2.374(2) Å for the Fe−Si bonds and 2.569(2)−2.615(2) Å for the Fe−Al distances. Switching the Si and Al positions gives rise to unreasonable bond lengths. The Fe−Si distances are short, considering the sum of the van der Waals radii (1.26 for Fe and 1.32 for Si), indicating significant bonding interactions between the Fe and neighboring Si atoms. Similar bond distances are observed in other iron silicides such as $ZrFe_4Si_2$ and $Yb_2Fe_4Si_9$.[35] Correspondingly, similar Fe−Al distances in the range of 2.53−2.72 Å are observed in many Fe/Al intermetallics.[36]

To describe this especially complex structure, it is useful to break it into layers perpendicular to the *c* axis. After understanding the structure of each layer, one can then illustrate how the layers stack and to what other elements they bind to form the overall three-dimensional structure. We note however that the structure is by no means lamellar. A basic repeating layer along the *ab* plane is shown in Figure 3. This perfectly flat slab composed of Al, Si, and Fe atoms repeats along the *c* axis at the unit cell repeat length of ∼4.1−4.2 Å. There

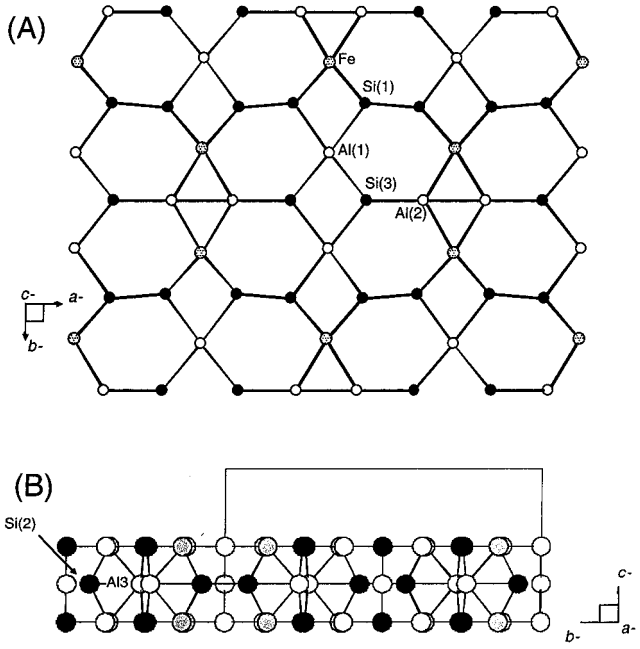

Figure 3. (A) Structure of the repeating layer along the *c* axis. (B) Two such layers rotated by 90° around the *b* axis to show the sandwiched Si(2) and Al(3) atoms.

are both single Al and Si atoms as well as Al−Al and Si−Si dimers within the layers. The latter Al(2)−Al(2), at 2.669(4) Å, and Si(1)−Si(1), at 2.364(2) Å, are parallel and bind to atoms, Fe, Al(1), and Si(3), to complete the

(35) $ZrFe_4Si_2$: Yarmolyuk, Ya. P.; Lysenko, L. A.; Gladyshevskii, E. I. *Dopov. Akad. Nauk Ukr. RSR, Ser A: Fiz. Tekh. Mat. Nauki* **1975**, *37*, 279 (b) $Yb_2Fe_4Si_9$: Gladyshevskij, E. I.; Bodak, O. I.; Jarovets, Ju. K.; Skolozdra, R. V. *Ukr. Fiz. Zh.* (Russian Edition) **1978**, *23* (1), 77−82.

(36) $REFe_2Al_{10}$: Tiede, V. M. T.; Ebel, T.; Jeitschko, W. J. *J. Mater. Chem.* **1998**, *8* (1), 125−130. (b) $ThFe_4Al_8$: Schäfer, W.; Will, G.; Gal, J.; Suski, *W. J Less-Common Met.* **1989**, *149*, 237−241.

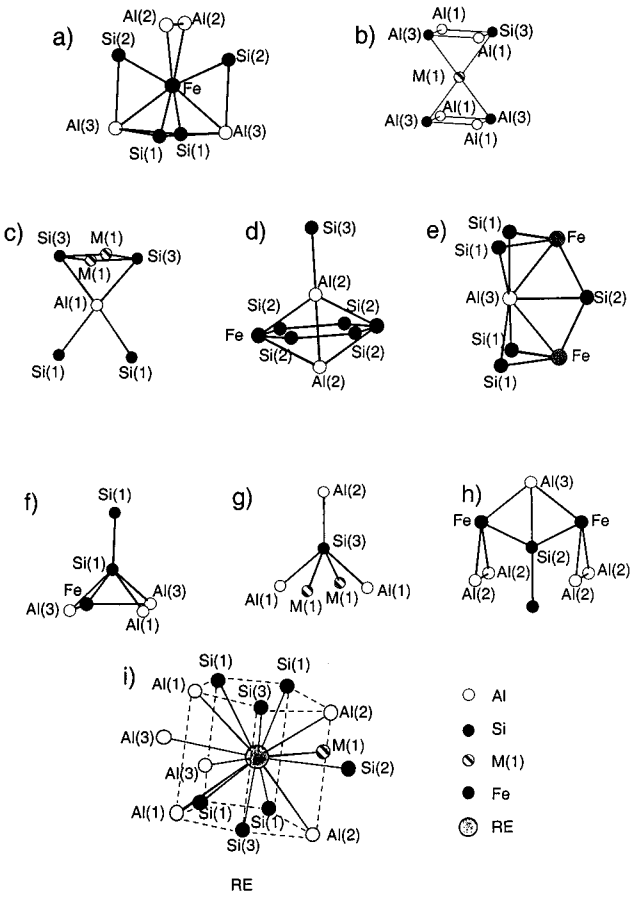

Figure 4. Coordination environments in $RE_4Fe_{2+x}Al_{7-x}Si_8$ (RE = Ce, Nd, Pr, Sm) of the individual atoms out to 3 Å, except for the RE atom, which is shown to 3.5 Å.

layer. As the layers stack along the *c* axis, they are joined with extra atoms found in the interlayer space, namely, Al(3), Si(2), and the mostly Al-containing mixed occupancy position M(1). The Si(2) atoms are found as dimers at a distance of 2.377 Å. As the extra interlayer atoms bond, the Fe atoms in the original layer (Figure 3) expand their coordination sphere from four to eight, bonding to both Al and Si atoms. This eight-coordinate Fe arrangement can be viewed as a result of two interpenetrating distorted tetrahedra of Si and Al atoms (see Figure 4a). The local coordination geometry of the mixed occupancy site M(1) is best described as a distorted square prism as the M(1) atom is sandwiched between two identical Si_2Al_2 rhombi (see Figure 4b). The M(1)−Al(1) and M(1)−Si(3) bond distances are 2.855(1) and 2.617(1) Å, indicative of Al−Al and Al−Si bonding.

The three pure Al sites in the structure exhibit several different bonding environments. Al(1) exhibits a slightly distorted square planar arrangement (Figure 4c), bonding to four separate Si atoms, while Al(2) (Figure 4d) exhibits a more distorted square planar arrangement bonding to another Al(2), two Fe atoms, and a Si(3) atom. Finally, Al(3) exhibits a higher coordination number of seven, in an arrangement that is best described as a distorted capped trigonal prism (Figure 4e).

The Si atoms exhibit both four- and five-coordinate environments. Si(1) and Si(3) exhibit distorted tetragonal pyramidal arrangements shown in Figure 4f and g. Si(1) bonding involves Fe, Al(1), two Al(3) atoms, and

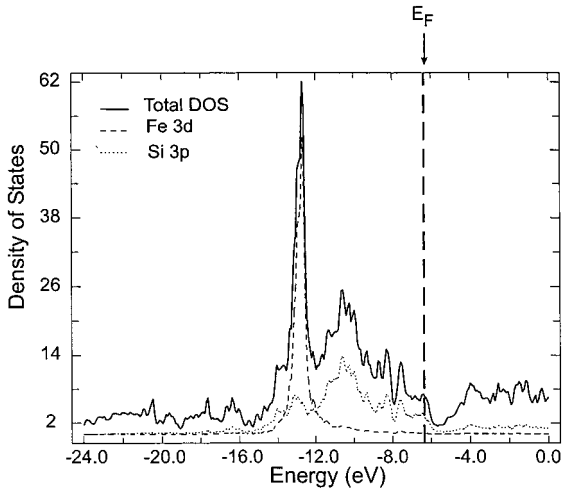

Figure 5. Total DOS for $Y_4Fe_2Al_7Si_8$ and contributions to the DOS of Fe 3d orbitals and Si 3p orbitals. The Fermi level is drawn in the dashed line for 162 valence electrons.

another Si(1) to form a dimer at 2.364(2) Å, while Si(3) binds to one Al(2), two Al(1) atoms, and two atoms of the mixed Al/Fe site M(1). The last Si atom, Si(2), exhibits a highly distorted square planar arrangement (Figure 4h), bonding to two Fe atoms, to Al(3), and also to another Si(2), forming the Si(2)−Si(2) dimer at 2.377(2) Å. Last, the rare earth atoms then reside within the channels parallel to the *c* axis in a 14-coordinate environment shown in Figure 4i.

Electronic Structure. Electronic band structure calculations were performed on the hypothetical, ordered, isostructural compound $Y_4Fe_2Al_7Si_8$. We were able to predict, from these calculations, the electrical and magnetic properties of these materials as well as obtain additional insight into the bonding and the charge distribution within the compound. In addition, a better understanding into the causes of the Al/Fe disorder in the M(1) position was sought.

The calculated electronic structure of $Y_4Fe_2Al_7Si_8$ suggests that it is a metal. Resistivity measurements on several crystals of the title compounds later confirmed the metallic behavior. A detailed look at the electronic structure highlights four different series of bands. One obvious set of weakly dispersed bands, lying close to the ionization potential energy of the Fe 3d orbitals, is primarily of Fe 3d character (90%). This band is feebly hybridized with Si 3p character (10%); see the density of states (DOS) in Figure 5. Below this manifold, between −24 and −14 eV, the bands show large dispersion due to the strong mixing between Si and Al 3s orbitals. The bands below the Fermi level and up to −12 eV consist primarily of Si 3p orbitals more or less mixed with Al 3p, Y 4d, and Fe 4p orbitals. This situation enables a certain degree of back charge transfer from the Si and/or Al atoms to the Y atoms and Fe atoms. Above the Fermi level, however, the bands are predominantly Y d character with slight hybridization with the 3p orbitals of Si and Al atoms, consistent with an oxidized Y atom.

Crystal orbital overlap population (COOP) analysis gives additional insights related to the bonding and its strength. For the majority of the COOP the Fermi level is situated below empty antibonding levels; consequently, these corresponding bonds are very strong and

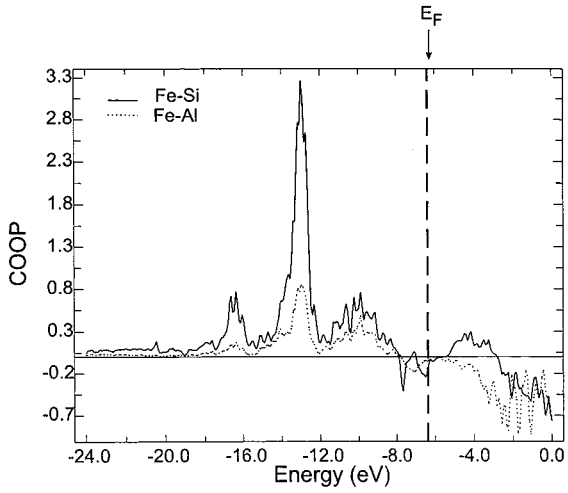

Figure 6. COOP curves corresponding to the Fe−Al and Fe−Si bonds. The Fermi level is shown in the dashed line.

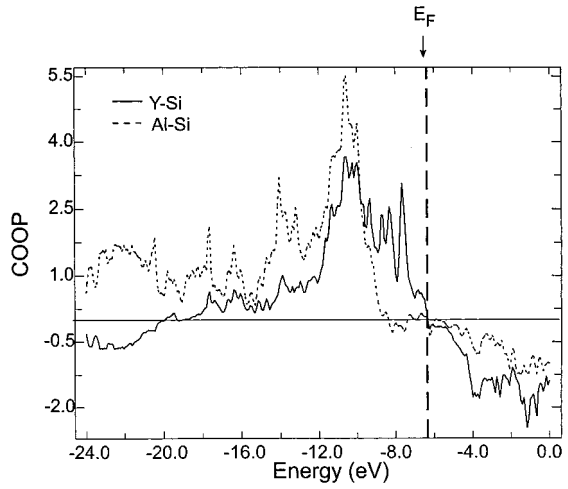

Figure 7. COOP curves for the Al−Si and Y−Si bonds. The Fermi level is shown in the dashed line.

therefore responsible for the compound's stability. However, for COOP corresponding to Fe−Al and Fe−Si bonds, the Fermi level lies close to a local antibonding maximum, making these two types of bonds least stable in the structure (see Figure 6). In $Y_4Fe_2Al_7Si_8$ the Fermi level crosses the bonding−antibonding boundary only in the Al−Si and Y−Si bonds as shown in Figure 7. This Fermi level location corresponds to a bonding optimization for these particular bonds. Overall, the fact that some antibonding levels were populated and that the Fermi level is located in a local maximum tend to slightly decrease the stability of the three-dimensional network.

If we consider the disordered compound $Y_4Fe_{2+x}Al_{7-x}Si_8$ in which the M(1) site in the 2d Wyckoff position is occupied by both Fe and Al, the total number of electrons will increase compared to the that of ideal $Y_4Fe_2Al_7Si_8$. It seems, consequently, probable that the Fermi level will fall in a valley (i.e., a pseudogap), in both the COOP and DOS curves, giving rise to a more stable configuration. It is tempting to suggest that these changes in electron count, brought about by the mixed occupancy in M(1), contribute to the strengthening of the Y−Al, Fe−Al, and Fe−Si interactions and consequently increase the stability of the structure. It would seem that the mixed occupancy at the M(1) site is actually necessary to form these compounds. This is an intriguing proposal as all experimental attempts to obtain stoichiometric samples free of this mixed occupied M(1) position have failed.

Table 7. Calculated Electron Densities for the $Y_4Fe_2Al_7Si_8$ Compound Corresponding to the Valence Electron Count

valence	electron density								
electrons	Y(1)	Fe	Si(1)	Si(2)	Si(3)	Al(1)	Al(2)	Al(3)	M(1)
162	1.78	11.36	4.46	4.45	4.74	2.26	1.99	2.07	2.26

Attempts to assign formal charges, based on the Mulliken populations, describe Fe as the most reduced element with a formal charge of −2 (electron densities 11.36 for 162 valence electrons). The silicon atoms Si(1), Si(2), and Si(3) have different formal charges of 0, 0, and −0.5, respectively. The "neutral" silicon atoms are consistent with the presence of homoatomic Si(1)−Si(1) and Si(2)−Si(2) bonds. In the crystal structure, Si(3) is completely surrounded by Al atoms (except for the presence of Fe atoms on the disordered site) and the difference in electronegativity between Al and Si could be responsible for the weak reduction of Si(3) (Pauling's electronegativity: 1.8 for Si and 1.6 for Al). As expected, the two most electropositive elements, Y and Al, are oxidized and their formal charges are +2 and +1, respectively, with no difference between the four types of Al. While we do not place much emphasis on the calculated numbers, other then to explore trends in charge distribution, it is reasonable that the rare earth metal holds a +3 formal charge. This is consistent with the high-temperature magnetic data (see below). Table 7 shows the corresponding calculated electron densities for the valence electron count of 162. Most likely, the real charge on the atoms will be different from the assigned formal charge. As mentioned above, the suggestion that the iron fills its 3d shell, resulting in a formal charge of −2, is reasonable and, qualitatively, the electron density distribution suggested by the calculations seems plausible.[37] The electron acceptor behavior is supported by the following: (a) the magnetic moment on the compounds being derived only from the rare earth atoms (see below); (b) Fe being one of the most electronegative elements in the structure (Pauling's electronegativity of 1.8); (c) Mössbauer spectroscopy (see below).[38]

Charge Transport Properties. Electrical conductivity and thermopower measurements on single crystals of $RE_4Fe_{2+x}Al_{7-x}Si_8$ (RE = Ce, Pr, Sm) were carried out over a temperature range of 5−300 K. The compounds exhibit metallic conductivity with values ranging from 12500 S/cm for the Pr compound to 6500 S/cm for the Sm analogue at room temperature (see Figure 8). Both the very high conductivity values and their temperature dependence agree with the metallic be-

(37) Vajenine, G. V.; Hoffmann, R. *J. Am. Chem. Soc.* **1998**, *120*, 4200−4208.

(38) A careful analysis of the crystal orbital coefficients for the iron atoms, of the slightly dispersed set of bands centered around −12.76 eV, indicated that the d_{xy}, d_{xz}, and d_{yz} orbitals remained pure, whereas the d_{z^2} and the $d_{x^2-y^2}$ orbitals tend to hybridize with the iron s and p orbitals. This hybridization is weak and can be represented by the schematic 0.9d + 0.07s + 0.03p for each of the d_{z^2} and $d_{x^2-y^2}$. To estimate the probability of an electron's presence on the different atomic orbitals of iron, one can consider that the three d pure Fe atomic orbitals are filled and consequently that they contain six electrons. To these six electrons, one has to add the 3.6 electrons coming from the two filled hybridized atomic orbitals of Fe.

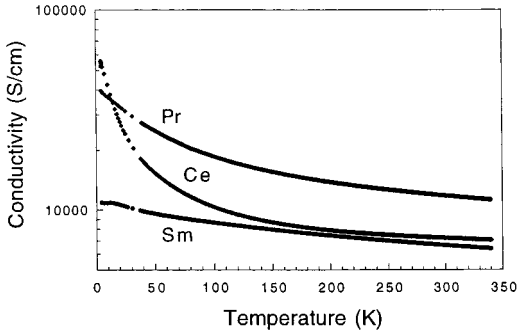

Figure 8. Electrical conductivity measurements of single-crystal samples of $Ce_4Fe_{2+x}Al_{7-x}Si_8$, $Pr_4Fe_{2+x}Al_{7-x}Si_8$, and $Sm_4Fe_{2+x}Al_{7-x}Si_8$, indicating metallic behavior.

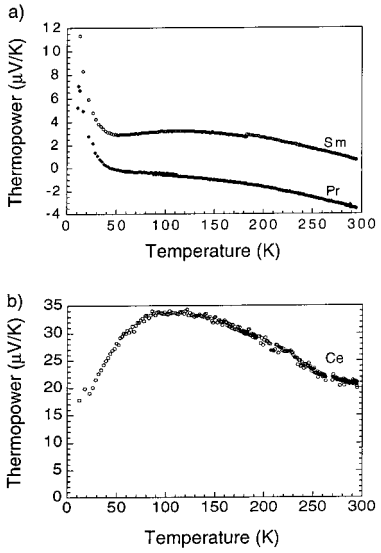

Figure 9. Thermopower measurements of (a) $Pr_4Fe_{2+x}Al_{7-x}Si_8$ and $Sm_4Fe_{2+x}Al_{7-x}Si_8$ and (b) $Ce_4Fe_{2+x}Al_{7-x}Si_8$. Values shown have been corrected for the contribution of the Au electrodes used to make contacts to the samples.

havior predicted from the electronic band structure calculations.

Thermopower values are small, on the order of a few μV/K, which is typical of metals in agreement with the predicted metallic behavior (see Figure 9). $Sm_4Fe_{2+x}Al_{7-x}Si_8$ exhibits positive thermopower values, that is, p-type behavior, with a general increase in value with decreasing temperature. The Pr analogue exhibits similar behavior with a gradual increase in values as the temperature decreases. The Pr analogue differs, however, in that the measured values at room temperature are negative and pass through zero, switching from n-type to p-type behavior, at about 50 K (Figure 9a). The rise in thermopower below 50 K is likely due to phonon drag effects that are common in metallic systems.

The Ce compound deviates markedly from the other two analogues by showing much larger thermopower values, which increase with decreasing temperature (see Figure 9b). The thermopower reaches a maximum of $+34$ μV/K, at $\sim$100 K, and then drops to lower values as the temperatures approaches 0 K. The presence of such maxima in the thermopower of metallic systems containing unpaired spins has been attributed in the past to Kondo effects[39] but further investigations are needed to study this issue further. Ce compounds are generally more prone to exhibiting Kondo behavior because of the f^1 electron configuration and the possibility of valence fluctuations associated with the $Ce^{3+/4+}$ coupling. Such fluctuations may be suggested by the magnetic susceptibility behavior at lower temperatures (see below). The thermopower maximum is reminiscent of similar maxima observed in a binary compound of Ce such as $CeAl_3$, $CeSn_3$, $CePd_3$, and $CePb_3$.[40]

Magnetic Properties. The magnetic properties of the title series, $RE_4Fe_{2+x}Al_{7-x}Si_8$ (RE = Ce, Pr, Nd, Sm), were investigated as a function of temperature. The low-temperature magnetic behavior (<15 K) is seemly dominated by a minor ferromagnetic impurity that has not been identified.

The high-temperature (T > 60 K) susceptibility data for all compounds, except for the Sm analogue, conforms to Curie−Weiss law behavior.[41] Graphs of these relationships, normalized to one rare earth atom per formula unit, are shown in Figure 10. From the Curie−Weiss law behavior a μ_{eff} for each rare earth atom was calculated. For $Pr_4Fe_{2+x}Al_{7-x}Si_8$ a value of 3.63 μ_B was obtained, which is very near the accepted experimental value of 3.40 μ_B for a Pr^{3+} ion.[42] The Ce and Nd analogues give μ_{eff} values of 2.52 and 3.31 μ_B, again very close to the accepted values of 2.28 and 3.50 μ_B for these RE^{3+} ions, respectively.

As observed in the charge transport properties, the magnetic properties of $Ce_4Fe_{2+x}Al_{7-x}Si_8$ differ from the other analogues as well, particularly in the region of 2 < T < 120 K. A significant change in slope of the $1/\chi_m$ curve occurs at temperatures $\approx$70 K, representing a deviation from Curie−Weiss behavior and a decrease in the μ_{eff} in this temperature region. The compound also exhibits a very large negative Weiss constant, θ of −195 K, when the data >150 K are fit to Curie−Weiss behavior. The reason for these anomalies is unclear, but they are similar in character to those observed in the susceptibility of $CeAl_3$ and $CeSn_3$. In the latter cases, the behavior was attributed to $Ce^{3+/4+}$ *valence fluctuations*. Studies are in progress on both the Mn and Co analogues[43] to probe these properties further.

The measured magnetic moments for all compounds described here clearly indicate that the rare earth atoms are in a 3+ state while the Fe atoms do not contribute to the overall magnetism. This absence of magnetic contribution from the Fe atoms could arise from substantial d-orbital electron filling, as mentioned above in the discussion of the band structure, and possible hybridization effects of the Fe d orbitals with neighboring Si atoms.

(39) $CePd_3B_x$: Houshiar, M.; Adroja, D. T.; Rainford, B. D. *Physica B* **1996**, 268−270. (b) $Ce_2T_3X_9$: Buschinger, B.; Trovarelli, O.; Weiden, M.; Geibel, C.; Steglich, F. *J. Alloys Compd.* **1998**, 633−636.

(40) Maple, M. B.; DeLong, L. E.; Sales, B. C. In *Handbook of the Physics and Chemistry of Rare Earths*; Gschneidner, K. A., Jr., Eyring, L., Eds.; North-Holland Publ. Co.: Amsterdam, The Netherlands, 1978; Chapter 11, pp 797−846.

(41) At this time no diamagnetic correction has been applied to the data because of the impurity presence. Such a correction is very small in comparison to the paramagnetic signal and will not meaningfully change the values of μ_{eff}.

(42) Bourdreaux, E. A.; Mulay, L. N. In *Theory and Applications of Molecular Paramagnetism*: John Wiley and Sons: New York, 1976.

(43) Our results on the Ce/Mn/Al/Si and Ce/Co/Al/Si systems will be published elsewhere.

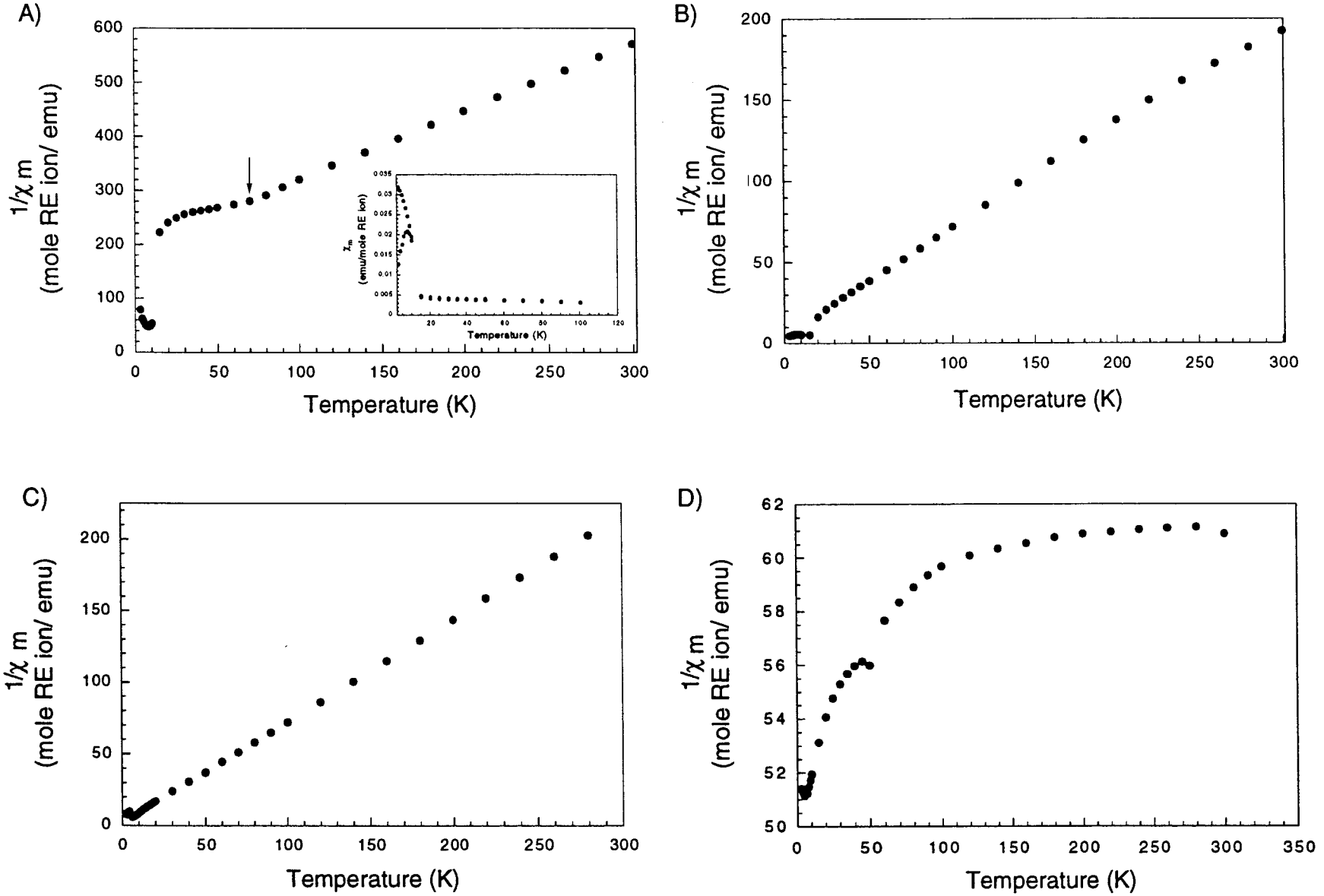

Figure 10. Magnetic susceptibility data for (a) $Ce_4Fe_{2+x}Al_{7-x}Si_8$, (b) $Pr_4Fe_{2+x}Al_{7-x}Si_8$, (c) $Nd_4Fe_{2+x}Al_{7-x}Si_8$, and (d) $Sm_4Fe_{2+x}Al_{7-x}Si_8$, standardized to one RE per formula unit, in a field of 200 G, exhibiting Curie−Weiss behavior. The calculated μ_{eff} from the data indicates that the RE is in a 3+ state while the Fe exhibits a noncontributing magnetic state. The arrow shown in the data of $Ce_4Fe_{2+x}Al_{7-x}Si_8$ marks the start of the deviation from Curie−Weiss behavior.

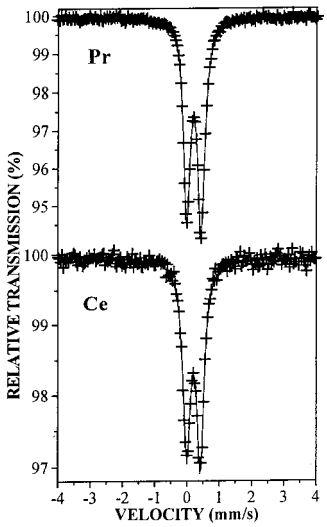

Figure 11. Typical Mössbauer spectra of $Pr_4Fe_{2+x}Al_{7-x}Si_8$ and $Ce_4Fe_{2+x}Al_{7-x}Si_8$ taken at 20 K. Velocity corresponds to the isomer shift (IS), which is referenced to Fe metal.

Table 8. Mössbauer Parameters, Collected at 20 K, of $RE_4Fe_{2+x}Al_{7-x}Si_8$ (RE = Ce, Pr)

	δ (mm/s)	ΔEq (mm/s)	$\Gamma/2$ (mm/s)	I_L/I_R[a]
Ce	0.31	0.42	0.14	0.94
Pr	0.315	0.45	0.13	0.90

[a] I_L/I_R = intensity of left line/intensity of right line.

A similar lack of magnetic contribution from Fe has been observed in other ternary rare earth iron compounds involving Al or Si, for example, in $REFe_2Al_{10}$[36a] and $Er_2Fe_3Si_5$.[44] In the latter only the rare earth atoms contribute to the observed magnetic moments. Compounds with diamagnetic rare earth elements, as in YFe_2Al_{10} or $LaFe_2Al_{10}$,[36a] exhibit only metallic Pauli paramagnetism.

$Sm_4Fe_{2+x}Al_{7-x}Si_8$ does not exhibit Curie−Weiss behavior at any temperature (see Figure 10d). This deviation is common in Sm^{3+} magnetism, which can be exceedingly complex, because of the thermal population of closely lying excited magnetic states.[42]

Mössbauer Spectroscopy. To probe further the electronic state of iron in $RE_4Fe_{2+x}Al_{7-x}Si_8$, we examined the Ce and Pr analogues with Mössbauer spectroscopy in the temperature region 4.2−300 K. We observed a classical quadruple doublet at all temperatures with no significant changes in the line widths of the quadruple doublets. Figure 11 shows a typical spectrum taken at 20 K. The spectra were analyzed by least-squares, fitting the quadruple doublet with Lorentzian lines. The best fitted values of the Mössbauer parameters are given in Table 8. The spectra show no evidence for magnetic splitting due to magnetic ordering of the Fe atoms. This is consistent with the aforementioned susceptibility measurements, which indicate that only the RE ions carry magnetic moments. Isomer shifts similar to those found here were observed in other Fe/Si compounds and alloys in which Fe has essentially zero magnetic moment. These cases include $REFe_2Si_2$,[45] $RE_2Fe_3Si_5$,[46] and β-$FeSi_2$.[47]

The Mössbauer spectra suggest that there is neither Fe 3d band magnetism nor Fe Curie−Weiss paramagnetism. The onset of 3d band magnetism as a result of Fe−Fe exchange interactions is not expected in these compounds because Fe−Fe distances are relatively large (4.080 Å) and the number of Fe nearest neighbors is only 2. Further evidence for the nonmagnetic character of Fe is provided by the values of the isomer shift of 0.21 mm/s at room temperature. This positive increase of the isomer shift relative to the value of metallic Fe relates to a decrease in the density of the s electrons at the Fe nucleus. This can be due either to a decrease in the number or to an enhanced screening of the 4s electrons in these compounds (brought about by the d-manifold electron filling as discussed above). In other words, the Fe atoms in $RE_4Fe_{2+x}Al_{7-x}Si_8$ *seem to be more reduced than those in Fe metal.* This is consistent with the expectation of electron flow from the electropositive RE and Al atoms to the more electronegative Fe atoms.

Concluding Remarks

With liquid Al as a solvent, the first quaternary compounds containing RE/Fe/Al/Si were discovered as part of a new isostructural series with the general formula of $RE_4Fe_{2+x}Al_{7-x}Si_8$ (RE = Ce, Nd, Pr, Sm). A unique site in the structure exhibits mixed Fe/Al occupancy and may be the key to the stability of the structure type. The compounds possess a novel structural arrangement and strongly metallic properties. The Ce analogue shows anomalies in the thermoelectric power and magnetism likely due to valence fluctuations. It is fascinating that in the materials the Fe atoms appear to be "highly reduced", an effect likely caused by electron transfer from the more electropositive atoms in the structure. The discovery of novel intermetallic compositions and structure types, in relatively refractory aluminum silicides, greatly underscores the value of liquid Al in the exploratory synthesis of new classes of materials.

Acknowledgment. Financial support from the Department of Energy (Grant # DE-FG02-99ER45793) is gratefully acknowledged.

Supporting Information Available: Tables of crystallographic details, atomic coordinates, isotropic and anisotropic displacement parameters for all atoms, and interatomic distances and angles for $RE_4Fe_{2+x}Al_{7-x}Si_8$ (RE = Ce, Pr, Nd, Sm) (PDF). This material is available free of charge via the Internet at http://pubs.acs.org.

CM0004937

(44) $Er_2Fe_3Si_5$: Moodenbaugh, A. R.; Cox, D. E.; Vining, C. B.; Segre, C. U. *Phys. Rev.* **1984**, *B29*, 109.

(45) Noakes, D. R.; Umarji, A. M.; Shenoy, G. K. *J. Magn. Magn. Mater.* **1983**, *39* (3), 309. (b) Umarji, A. M.; Noakes, D. R.; Viccaro, P. J.; Shenoy, G. K.; *J. Less-Common Met.* **1983**, *94* (2), 265−265.

(46) Noakes, D. R.; Shenoy, G. K.; Niarchos, D.; Umarji, A. M.; Aldred, A. T.; *Phys. Rev. B* **1983**, *27* (7), 4317.

(47) Fanciulli, M.; Rosenblad, C.; Weyer, G.; Svane, A.; Christensen, N. E.; vonKanel, H.; Rodriguez, C. O. *J. Phys.: Condens. Matter* **1997**, *9* (7), 1619. (b) Szymanski, K.; Dobrzynski, L.; Satula, D.; Greneche, J. M. *J. Phys.: Condens. Matter* **1997**, *9* (18), 3793.